Ultrasonics 91 (2019) 193–200

Contents lists available at ScienceDirect

Ultrasonics

journal homepage: www.elsevier.com/locate/ultras

Study on contact performance of ultrasonic-assisted grinding surface

Wen Yuqin[a,*], Tang Jinyuan[a], Zhou Wei[b], Zhu Caichao[c]

[a] State Key Laboratory of High Performance Complex Manufacturing, Central South University, Changsha, Hunan, China
[b] Intelligent Manufacturing Institute of HUNST, Hunan University of Science and Technology, Xiangtan, Hunan, China
[c] State Key Laboratory of Mechanical Transmission, Chongqing University, Chongqing, China

ARTICLE INFO

Keywords:
Ultrasonic-assisted grinding
Micromorphology
Contact stiffness
Contact pressure

ABSTRACT

The contact performance of ultrasonic-assisted grinding surface is studied in this paper. An improved simplified model of rough surface profile is proposed to find the microscopic feature parameters, such as the curvature radius of the asperity, which are suitable for contact analysis and calculation. Then a more accurate rough surface contact analysis model is obtained by combining the classical ZMC contact model. Based on the contact analysis model, the contact mechanism of ultrasonic-assisted grinding surface is studied. The contact stiffness and local maximum contact pressure of the surfaces under different cutting depths and ultrasonic amplitudes are calculated, and the correlation rule between the parameters of ultrasonic-assisted grinding and the contact performance of the machined surface is obtained: (1) With the increase of the cutting depth, the surface roughness of the workpiece increases; under the same load, the contact stiffness decreases and the maximum local contact pressure increases. (2) With the increase of the ultrasonic amplitude, the surface roughness of the workpiece first decreases and then increases. Under the same load, the contact stiffness increases first and then decreases, while the maximum local contact pressure resents an opposite variation trend. Under the experimental conditions, the surface contact performance of the workpiece is the best when the ultrasonic amplitude is 4 μm. Additionally, the contact performance of the ultrasonic-assisted grinding surface and the conventional grinding surface is compared: (1) When the ultrasonic amplitude is 4 μm, the surface roughness of the workpiece is at least 24% lower than that of the conventional grinding surface. (2) Under the same load, the surface contact stiffness of the ultrasonic-assisted grinding surface is increased by at least 68%, and the maximum local contact pressure is reduced by at least 17%. It is found that the interference motion of abrasive particles in the ultrasonic-assisted grinding process makes the surface height distribution more concentrated and the density of asperity increased, which results in a better contact performance compared with the conventional grinding surface.

1. Introduction

The surfaces of mechanical parts are uneven at the micro level, characterized by a series of discretely distributed contact areas, and the real contact area which is only part of the smooth nominal contact area is far smaller than the nominal contact area. The real contact area and the contact pressure of the contact surface directly affect the bearing capacity, friction, wear, fatigue and other properties of the transmission parts [1–4]. For example, the existence of rough surface decreases the local stiffness of a mechanical structure, which directly affects the static and dynamic characteristics of the structure, and meanwhile increases the local contact pressure, which directly affects the fatigue life.

Ultrasonic-assisted grinding is a grinding process formed by applying ultrasonic vibration during the traditional grinding process. In ultrasonic-assisted grinding, the effects of micro differentiation, rigidity, cutting edge sharpening, cavitation, and stress and energy concentration will be produced [5], which can decrease the grinding force [6] and grinding temperature [7], reduce wheel blockage and wheel wear and improve the integrity of the machined surface [8]. Therefore, ultrasonic-assisted grinding has always been a hot spot of research.

The workpiece with ultrasonic-assisted grinding has different surface features from the conventional grinding workpiece. Xue [9] studied the ultrasonic-assisted grinding of high performance alloy with the electroplated grinding wheel. It was found that under certain conditions, the mesh microstructure appeared on the surface of ultrasonic-assisted grinding and that the mesh microstructure showed different characteristics under different processing parameters. It was observed by Chen [10] that the increase of ultrasonic amplitude decreased the lateral bulge of the mesh microstructure, increased the interference

* Corresponding author.
E-mail address: yuqinwen@csu.edu.cn (Y. Wen).

https://doi.org/10.1016/j.ultras.2018.08.009
Received 15 March 2018; Received in revised form 2 July 2018; Accepted 13 August 2018
Available online 14 August 2018
0041-624X/

degree of adjacent grains, and decreased the surface roughness. In recent years, researchers have focused mainly on the relationship between parameters of ultrasonic-assisted grinding and surface roughness of workpiece [11–13]. However, the actual contact performance of ultrasonic-assisted grinding surfaces under the micro morphology has not been deeply investigated.

In order to study the contact performance of mechanical parts under micromorphology more accurately and intensively, the rough surface contact model based on statistics theory has been widely studied. Greenwood and Williamson [14] first proposed a rough plane contact model considering the elastic deformation of the asperity (the GW model), but the GW model is limited to the assumption of pure elastic deformation. Zhao et al. [15] used the method of interpolation to establish a surface contact model (ZMC model) which considers all the three states: the fully elastic deformation, elastic-plastic deformation and fully plastic deformation. With constant revisions and improvements, the contact model of rough surfaces based on statistics has been widely used in rough surface contact analysis. The height distribution, curvature radius and density of the asperity become the main modeling parameters. However, studies by Whitehouse and Archard [16] have found that the curvature radius and density of asperity calculated by the stochastic process theory cannot represent the intrinsic property of the surface, but depend on the sampling interval. Greenwood [17] proposed that the original definition method of asperity peak cannot reasonably describe the surface asperity, especially when the sampling interval is very small. In the analysis of contact between the actual machined rough surfaces, considering that the surface morphology measured by the optical instrument is affected by the sampling interval [18], the average curvature radius of the asperity calculated by the classical three-point method is usually too small so that it is not suitable for calculation of rough surface contact model.

It can be found from the analysis of existing researches that the following problems need to be studied further: (1) the relationship between the surface micromorphology of the workpiece of the ultrasonic-assisted grinding and the contact performance; (2) the relationship between the parameters of ultrasonic-assisted grinding and the contact performance of the machined surface; (3) comparison of contact performance between surfaces of ultrasonic-assisted grinding and surfaces of conventional grinding. An improved simplified model of rough surface profile is proposed in this paper and the measured micromorphology data of ultrasonic-assisted grinding surface is simplified to find the microscopic feature parameters, such as the curvature radius of the asperity, which are suitable for contact analysis and calculation. The contact stiffness and local maximum contact pressure of the surfaces under different cutting depths and ultrasonic amplitudes are calculated by combining the classical ZMC contact model, and the correlation rule between the parameters of ultrasonic-assisted grinding and the contact performance of the machined surface is obtained. The contact performance of the ultrasonic-assisted grinding surface and the conventional grinding surface is compared, and the mechanism of improvement on contact performance of ultrasonic-assisted grinding surface is studied.

2. Improved simplified model of micro surface profile

To solve the contact problem of rough surfaces, statistical models have been modified and improved. So far, these models have been widely used in rough surface contact analysis. However, important modeling parameters, such as the curvature radius and density of asperity, cannot be directly measured by measuring instruments. Usually, researchers adopt the 3-point method to define the asperity peaks and calculate the radius of curvature and the density of asperity. Considering that the surface morphology measured by the optical instrument is affected by the sampling interval, the average curvature radius of the asperity calculated by the classical three-point method is usually too small and is influenced by the sampling interval so that it is not suitable for calculation of rough surface contact model. Based on the literature [19], a new method of asperity definition based on the reference line and the height of peak and valley is proposed in this paper. The real profile of the rough surface is described by parabolas and they are simulated by ensuring the minimum least square error between the parabolas and the real profile. The surface profile of the workpiece is measured by the optical profilometer, and the discrete points of the surface profile of the workpiece are obtained. Considering the groove characteristics of the grinding surface, the two-dimensional profile in the vertical groove direction is simplified by parabolas, so as to facilitate further contact analysis of the surface of the ultrasonic-assisted grinding.

2.1. Definition method of asperity

Using tools such as a white light interferometer, the discrete point height sequence of the profile of rough surface $z(i)$ is obtained. The average height line of the surface h_0 is calculated, and it is taken as the reference line.

$$h_0 = (1/N)\sum_{i=1}^{N} z_i \tag{1}$$

In the equation, N is the total number of the discrete points of the surface profile.

According to the relationship between the measured profile and the reference line, the continuous discrete points which are higher than the reference line are regarded as a same asperity, and the discrete points of the profile are simplified by a parabola. The simplified sketch of the parabolic asperity is shown in Fig. 1.

As indicated by the new problem found by Kucharski et al. [20], the location of the reference line will have a huge impact on the simplified results in the method mentioned above. As shown in Fig. 2, the discrete points in the figure are all higher than the reference line. If the discrete points are divided by the reference line only, they will be defined as one asperity for simplification. However, it is obvious that, in the case shown in the figure, the simplification error will be smaller if the discrete points are divided into two asperities.

In the rough surface profile, peak points and valley points are important features which can be determined easily. Therefore, the division method is discussed by considering the ratio between the height of the valley point and the height of the peak point. The results show that when the ratio between the height of the valley point and the height of the peak point is less than 0.5, the simplification error of dividing into two asperities is invariably lower than the simplification error of dividing into one asperity. Therefore, in order to reduce the simplification error and simplify the rough surface profile more accurately, on the

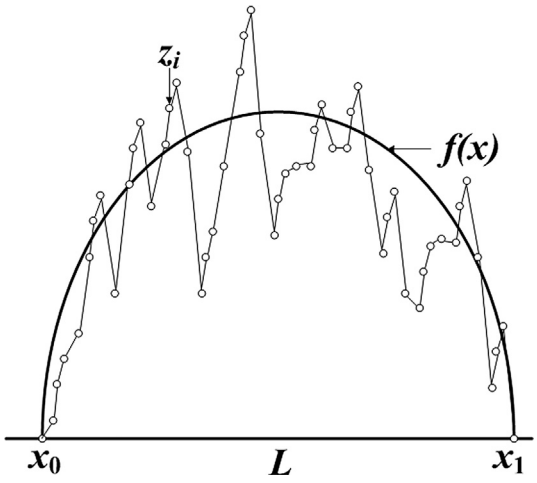

Fig. 1. Simplified sketch of parabolic asperity.

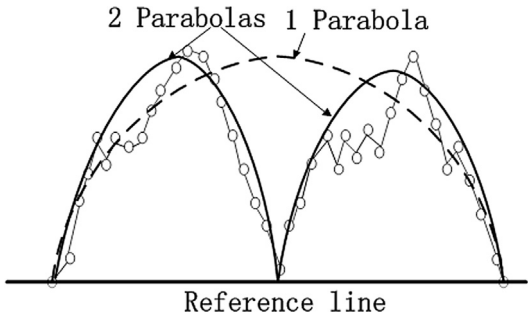

Fig. 2. Schematic diagram for division of asperities.

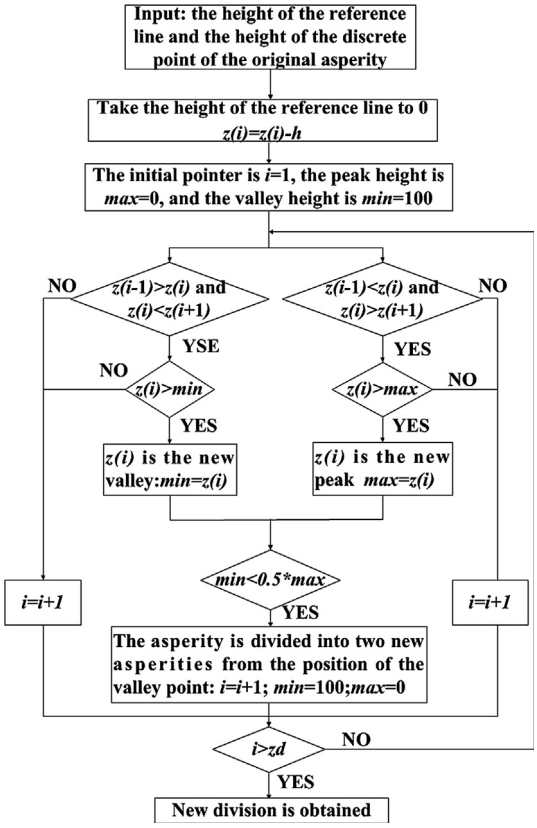

Fig. 3. Flow chart of asperity division.

basis of the method of dividing the asperity with the reference line, the corresponding discrete points are divided into a new asperity if the ratio between the height of the valley point and the height of the peak point is less than 0.5. If the height of the discrete points $z(i) > z(i+1)$ and $z(i) > z(i-1)$, this point is the peak point. Similarly, if the height of the discrete points $z(i) < z(i+1)$ and $z(i) < z(i-1)$, this point is the valley point. The flow chart of the improved division method is shown in Fig. 3.

2.2. Asperity simplification and parameter calculation

For a defined asperity, if its profile intersects the reference line at point x_0 and x_1, let the parabola be $z = f(x)$, then the parabolic equation is expressed as:

$$z = f(x) = q(x-x_0)(x-x_1) + h_r \tag{2}$$

where q is the coefficient of the parabolic function, and h_r is the height of the reference line.

Based on the results of Ciulli et al. [19], the best simplified model can be obtained with the least square approximation. The least mean square error of parabola Er is determined by the following equation:

$$Er = \sum_{i=1}^{n} [z_i - h - q(x_i - x_0)(x_i - x_1)]^2 \tag{3}$$

The coefficient of the parabolic function q can be obtained by making the derivative $\partial Er/\partial q$ equal to zero, giving:

$$q = \frac{\sum_{i=1}^{n} z_i [x_i^2 - (x_0 + x_1)x_i + x_0 x_1]}{\sum_{i=1}^{n} [x_i^2 - (x_0 + x_1)x_i + x_0 x_1]^2} \tag{4}$$

The radius of curvature of the simplified asperity R is calculated by the following equation:

$$R = \frac{1}{2\,|q|} \tag{5}$$

3. Rough surface contact analysis model based on simplified method

After the profile of rough surfaces is simplified, the geometrical parameters, such as the curvature radius of asperity which is suitable for contact analysis, can be obtained, and then the contact state of the surface can be calculated and analyzed by combining the mechanical properties of the material and the relevant contact mechanics model.

The curvature radius and height of the asperity are obtained based on the simplified method of the profile. Then the contact state of the whole surface can be obtained by calculating the contact of each asperity.

3.1. Contact model of asperity

According to Hertz contact theory and the theory of Zhao et al. [15], the deformation of a single asperity is divided into three stages, namely, completely elastic stage, elastic-plastic stage and completely plastic stage, and then the elastic-plastic contact model of the asperity is obtained. As shown in Fig. 4, the deformation of a single asperity when in contact with a plane is divided into three stages, i.e. completely elastic, elastic-plastic and completely plastic stages, and the boundary condition is the normal deformation of the asperity ω which is determined by the following formula:

$$\omega = z - h \tag{6}$$

where z is the height of the asperity, and h is the average distance between the surfaces.

(1) Completely elastic stage ($\omega < \omega_1$):

Real contact area:

$$A_1 = \pi R \omega \tag{7}$$

Average contact pressure:

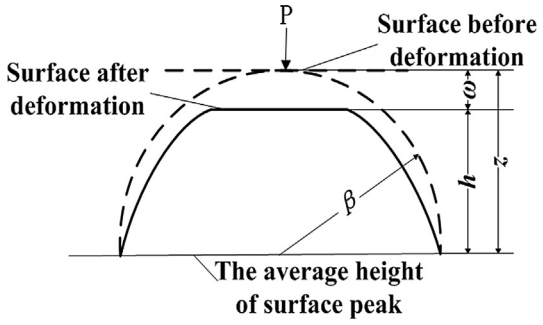

Fig. 4. Contact of a single asperity with a rigid smooth surface.

$$p_1 = \frac{4E}{3\pi}\left(\frac{\omega}{R}\right)^{1/2} \tag{8}$$

where ω_1 = the critical normal deformation of the initial yield point, E = the elastic modulus, R = radius of the asperities.

(2) Completely plastic stage ($\omega > \omega_2$):

Real contact area:

$$A_3 = 2\pi R\omega \tag{9}$$

Average contact pressure:

$$p_3 = H \tag{10}$$

where ω_2 = the critical normal deformation of the complete plastic deformation point, H = the hardness of the softer material.

(3) Elastic-plastic stage ($\omega_1 < \omega < \omega_2$):

$$\text{Real contact area: } A_2 = \pi R\omega[1 + f(\omega)] \tag{11}$$

$$\text{Average contact pressure: } p_2 = kH\left(\frac{\omega}{\omega_1}\right)^{1/2} \times [1-f(\omega)] + Hf(\omega) \tag{12}$$

$f(\omega)$ is the interpolation function and

$$f(\omega) = -2\left(\frac{\omega - \omega_1}{\omega_2 - \omega_1}\right)^3 + 3\left(\frac{\omega - \omega_1}{\omega_2 - \omega_1}\right)^2 \tag{13}$$

H is the hardness of the softer material, and its value is about 2.8 times of the yield strength of the material; k is the average contact pressure coefficient, and its value is related to Poisson's ratio of the softer material [21]. The critical normal deformation of the initial yield point and the critical normal deformation of the complete plastic deformation point are determined by the following formulas [15]:

$$\omega_1 = \left(\frac{3\pi kH}{4E}\right)^2 R \tag{14}$$

$$\omega_2 = 110\omega_1 \tag{15}$$

3.2. Rough surface contact model

As shown in Fig. 5, the contact between two rough surfaces can be replaced by the contact between a rough surface and a rigid smooth surface. Accordingly, the contact between a rough surface and a rigid smooth surface is considered. For each simplified asperity, the contact length L_i is determined by the following formula:

$$L_i = 2\sqrt{\frac{A_i}{\pi}} \tag{16}$$

As shown in Fig. 5, for a given surface contact distance h, according to Eqs. (6)–(15), the average contact pressure p_i and the contact area A_i of each asperity can be calculated. Therefore, the total contact length and the total load can be obtained by superimposing the results of each asperity. For comparison, the total contact length per unit width L_t^* and the total load per unit width W_t^* is computed according to the profile length L_t:

$$L_t^* = \frac{\sum L_i}{L_t} \tag{17}$$

$$W_t^* = \frac{\sum L_i p_i}{L_t} \tag{18}$$

Considering the contact between a rough surface and a rigid smooth surface, the equivalent elastic modulus is determined by the following formula:

$$E' = \frac{E}{1-\nu^2} \tag{19}$$

where E is the elastic modulus of the material, and ν is the Poisson's ratio of the material.

The maximum local contact pressure is determined by the following formula since the contact state of each asperity in contact can be obtained:

$$p_{\max} = \max\{p_i\} \tag{20}$$

The normal contact stiffness is the ability to resist the normal deformation of the joint under the external force. In the rough surface contact model, the normal contact stiffness of the joint is the ratio of the normal load increment to the normal deformation increment. Therefor, the contact stiffness per unit width K is:

$$K = \frac{dW_t^*}{-dh} \tag{21}$$

4. Calculation and analysis of contact performance of ultrasonic-assisted grinding

4.1. Experiment and measurement

In order to compare the difference in contact performance between the ultrasonic-assisted grinding surface and the conventional grinding surface, and explore the correlation rule between the ultrasonic amplitude and the contact performance of the machined surface, four groups of plane workpiece are studied, which are conventional grinding (amplitude = 0 μm) and ultrasonic-assisted grinding (amplitude = 4 μm, 7 μm, 10 μm). To ensure the rationality and scientificity of the law, each group contains three workpieces under different depths of cut (depth of cut = 5 μm, 15 μm, 25 μm). The machine tool used in the experiment is VMC850E vertical machining center. Ultrasonic-assisted grinding equipment is an ultrasonic-assisted grinding system for general machine tools developed in cooperation. Fig. 6 shows the process of ultrasonic-assisted grinding with the experimental equipment (see Table 1).

The micromorphology data of the workpiece surface is measured by the white light interferometer Wyko NT9100. Fig. 7 shows the surface

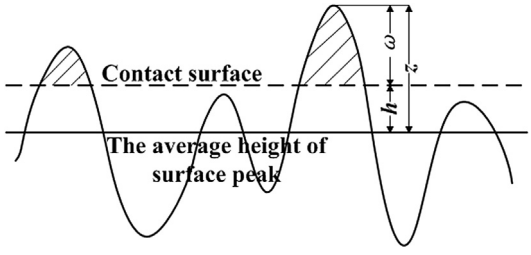

Fig. 5. Contact between a rigid smooth plane and a rough plane.

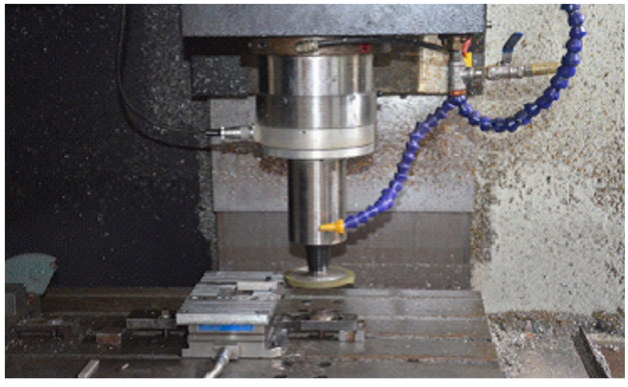

Fig. 6. Experimental equipment for ultrasonic-assisted grinding.

Table 1
Major machining parameters.

Grinding wheel	CBN (the grit size of 120)
Radius of grinding wheel	100 mm
Workpiece	12CrNi4A (9 × 9 × 16 mm)
Grinding conditions	Wheel velocity 1500 r/min; workpiece velocity 200 mm/min; depth of cut 5–25 μm
Grinding process	Surface grinding
Coolant	120 l/mim, emulsion (Castrol Syntilo 2000)
Direction of ultrasonic vibration	Cross feed direction
Ultrasonic vibration conditions	Frequency 20 kHz; amplitude 0–10 μm

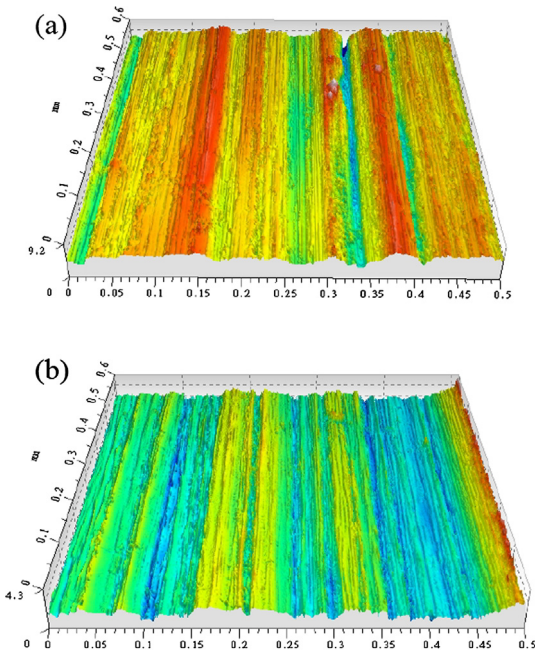

Fig. 7. Surface micromorphology (a) common grinding; (b) ultrasonic-assisted grinding (amplitude of 4 μm).

morphology of the ultrasonic-assisted grinding surface and the common grinding surface when the depth of cut is 5 μm.

4.2. Calculation of contact performance

Considering the groove characteristics of the grinding surface, the two-dimensional profile in the vertical groove direction is simplified by parabolas based on the improved simplified model of rough surface profile. Then the micromorphology parameters such as the curvature radius and height of the asperity of the grinding workpiece surface are obtained. The example of local enlargement of simplified surface profile is shown in Fig. 8.

Fig. 8 shows the effectiveness of the simplified method. The surface height is dimensionless, and the ordinate of the figure is z/σ. The standard deviations of height distribution σ of two surfaces are 1.35 μm and 0.51 μm respectively, so the actual difference of height distribution and roughness of the two profiles is very large. The profile (a) is much more rough. Besides, the distribution of the asperities on the profile (b) is more uniform, and there are fewer deep valley and high peaks on the profile (b).

The relation between the surface roughness of the workpiece and the machining parameters is shown in Fig. 9. It can be seen that the surface roughness of the workpiece increases with the increase of the cutting depth, which is in line with the change law of the surface roughness of the workpiece under the grinding process. Under the same

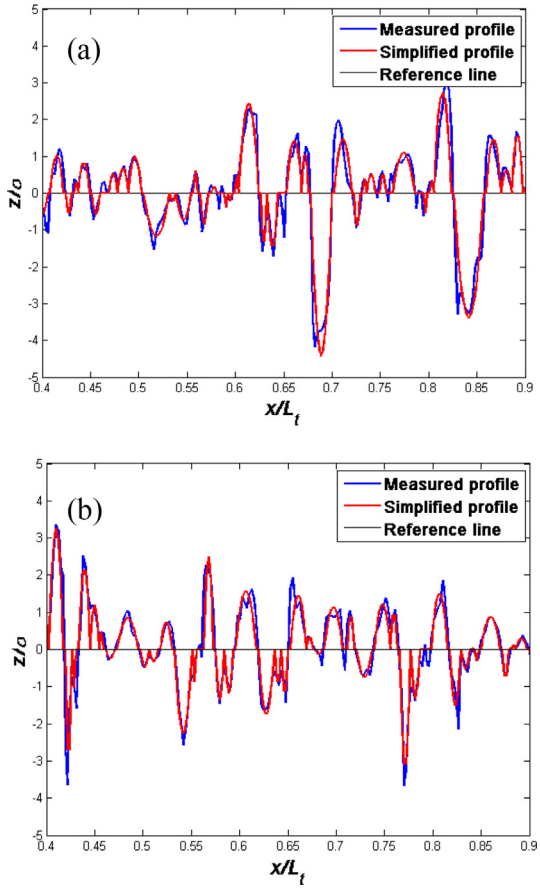

Fig. 8. Simplification of surface profile (a) common grinding; (b) ultrasonic-assisted grinding (amplitude of 4 μm).

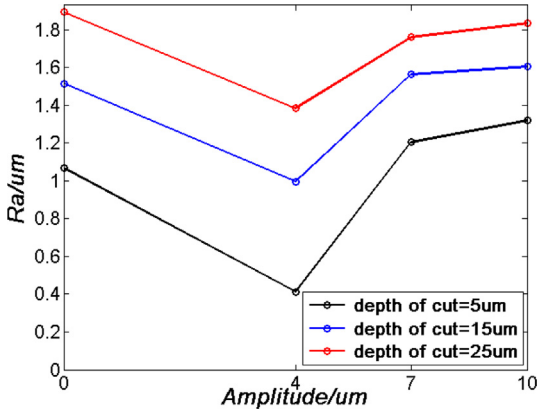

Fig. 9. Relationship between roughness and machining parameters.

cutting depth, the surface roughness of the workpiece decreases first and then increases with the increase of the ultrasonic amplitude. When the amplitude is large, the surface roughness of the workpiece will be even higher than that of the ordinary grinding surface. In general, ultrasonic vibration can improve the surface properties of workpiece, but the amplitude is not the bigger the better. The axial ultrasonic vibration is added to the machining process, but because of the large wheel, Poisson effect will be generated, which will cause additional radial vibration. The radial vibration will hammer the surface of the workpiece and cause additional damage. When the amplitude is large, the radial vibration will also be large, which will cause damage to the surface. So it will increase the surface roughness when the amplitude is large. Chen et al. [12,22] has also studied related issues. Therefore,

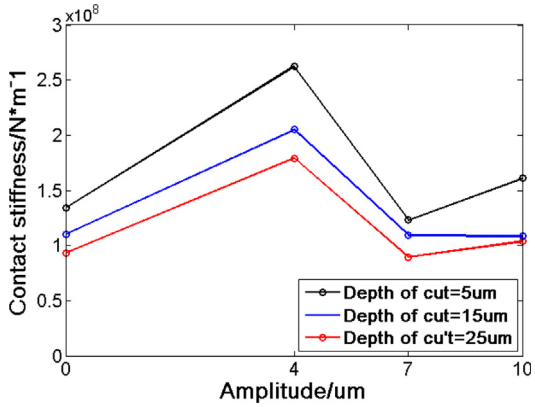

Fig. 10. Relation between surface contact stiffness and machining parameters.

under different processing parameters and different processing conditions, there may be a most suitable amplitude and the smallest roughness can be obtained. Under the three sets of cutting depth, the surface roughness of the workpiece under the ultrasonic amplitude of 4 μm is the smallest, which is 59%, 29% and 24% lower than the surface roughness of the commom grinding workpiece, and the smaller the cutting depth is, the better the effect of surface improvement is.

Based on the simplified profile of the workpiece, the contact calculation and analysis of each work piece are carried out according to the method proposed in this paper. For the convenience of comparison, the contact stiffness and the maximum local contact pressure of each piece of workpiece under constant unit area load are calculated. P = 100 N is taken to calculate the contact stiffness and the maximum local contact pressure on the area of 1 mm^2, and the comparison is made. In order to ensure the accuracy of the results, all the profiles at the vertical groove direction obtained from measurements on 1 mm^2 are calculated, and the average value is obtained for the final result. The relation between the surface contact stiffness and the machining parameters is shown in Fig. 10. The relationship between the local maximum contact pressure and the machining parameters is shown in Fig. 11.

As shown in Fig. 10, with the increase of the cutting depth, the contact stiffness of the workpiece surface is reduced. Under the same machining parameters, the surface contact stiffness of the ultrasonic grinding is almost all higher than that of the commom grinding surface, which indicates a better load carrying capacity.

As shown in Fig. 11, for the commom grinding surface, the maximum local contact pressure increases with the increase of the depth of cut. For the ultrasonic-assisted grinding surface, the change of the maximum local contact pressure is disorderly when the amplitude is

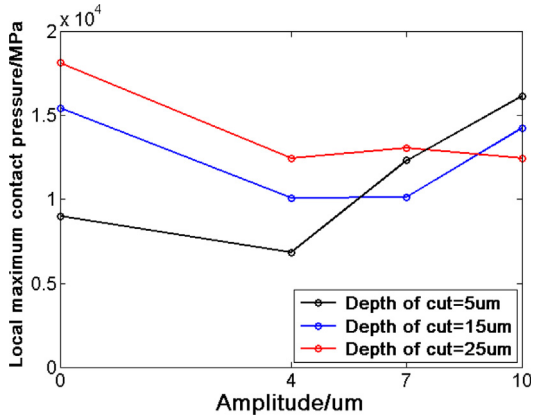

Fig. 11. Relationship between local maximum contact pressure and machining parameters.

larger and the depth of cut is smaller. Under the experimental conditions, the maximum local contact pressure of the workpiece surface with the ultrasonic amplitude of 4 μm is the smallest, which is 17%, 28% and 30% lower than that of the commom grinding surface, and the larger the depth of cut is, the more obvious the reduction effect is.

5. Mechanism analysis of difference in surface contact performance

Through calculation and comparison of the contact performance, it is known that under proper machining parameters, the contact performance of the ultrasonic-assisted grinding surface is more optimum because of low roughness, high contact stiffness and low wear. In order to further study the causes of the difference in contact performance, combined with the surface generation mechanism of ultrasonic-assisted grinding, the difference between ultrasonic-assisted grinding surface and common grinding surface is analyzed from two aspects: the height distribution of surface and the distribution of asperities. The calculation results show that the difference of the contact performance between the ultrasonic-assisted grinding surface and the common grinding surface is the greatest when the ultrasonic amplitude is 4 μm. Therefore, this section mainly compares the ultrasonic-assisted grinding surface under this condition and the commom grinding surface.

5.1. Analysis of surface height distribution

The height distribution of the rough surface has a direct influence on the contact and wear properties of the surface. Under the same normal deformation, the height distribution of rough surface directly affects the actual contact area. The more concentrated the surface height is, the better ability to resist deformation and wear the surface will have. Fig. 12 shows the height probability density distribution of ultrasonic-assisted grinding surface and commom grinding surface under different depths of cut.

As shown in Fig. 12, under the same cutting depth, the height distribution of the ultrasonic-assisted grinding surface is more concentrated than that of the common grinding surface. This shows that under the same normal deformation, ultrasonic vibration assists the grinding surface with greater bearing length ratios. That is to say, under the same nominal contact area, the actual contact area of the ultrasonic-assisted grinding surface is larger so that the surface has a stronger ability to resist deformation and a larger contact stiffness, which is consistent with the calculation results of contact stiffness.

5.2. Analysis of asperity distribution

In addition to the surface height distribution, the asperity distribution also affects the surface contact performance. Under the same

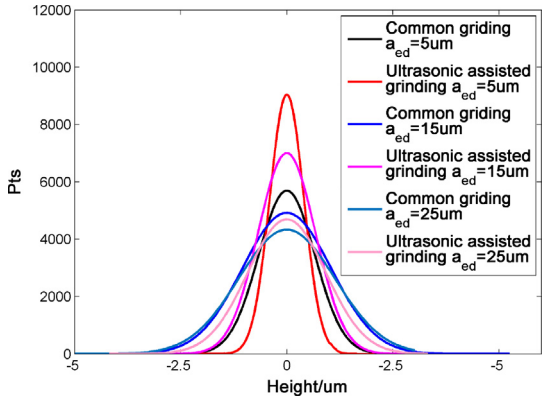

Fig. 12. Height probability density distribution of ultrasonic-assisted grinding surface and commom grinding surface.

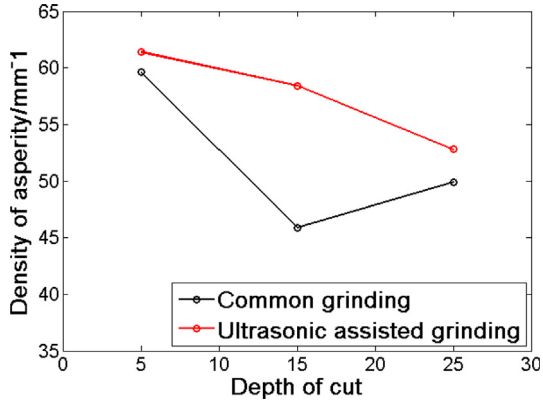

Fig. 13. Asperity density of ultrasonic-assisted grinding surface and commom grinding surface.

load, the more the asperities are involved in contact, the more uniform distribution of contact pressure is and the better the contact fatigue performance of the surface is. Based on the proposed simplified model of rough surface profile, the density of asperities on different workpiece surfaces is calculated. Fig. 13 shows the density of asperities on the ultrasonic-assisted grinding surface and the common grinding surface under different cutting depths.

As can be seen from Fig. 13, under the same cutting depth, the density of asperities of the ultrasonic-assisted grinding surface is greater than that of the common grinding surface. This shows that under the same load, more asperities of the ultrasonic-assisted grinding surface will be in contact, the pressure distribution is more uniform and the maximum contact pressure can be reduced effectively. Accordingly, the surface has a better contact fatigue performance, which agrees with the calculation results of the maximum local contact pressure.

The interference motion of abrasive particles in the ultrasonic-assisted grinding process is the main reason for the difference of the surface height distribution and the distribution of asperities. Fig. 14 shows the contrast of grinding trajectories of abrasive particles in the ultrasonic-assisted grinding process and common grinding process. As shown in Fig. 14, during the common grinding process, the abrasive particles are moving in a straight line with the surface of the workpiece. However, during the ultrasonic-assisted grinding process, the abrasive particles have sinusoidal movement relative to the surface of the workpiece. The interference motion of abrasive particles leads to more asperities on the grinding surface, which makes the surface pressure distribution more uniform and reduces the peak of local maximum contact pressure.

In order to show the influence of the interference motion of abrasive particles on the surface topography more clearly, the surface topography of the ultrasonic-assisted grinding is added as shown in Fig. 15. It can be seen from the figure that the surface of ultrasonic-assisted grinding has obvious special crosshatch microstructure, which is caused by the interference motion of abrasive particles.

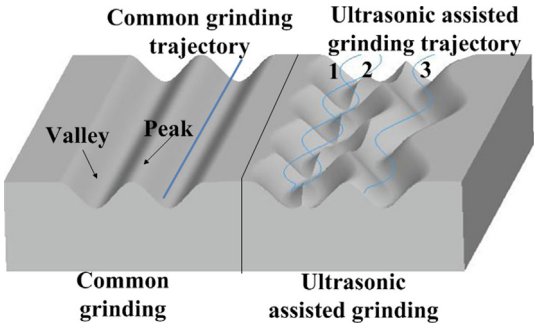

Fig. 14. Comparison of grinding trajectories of abrasive particles.

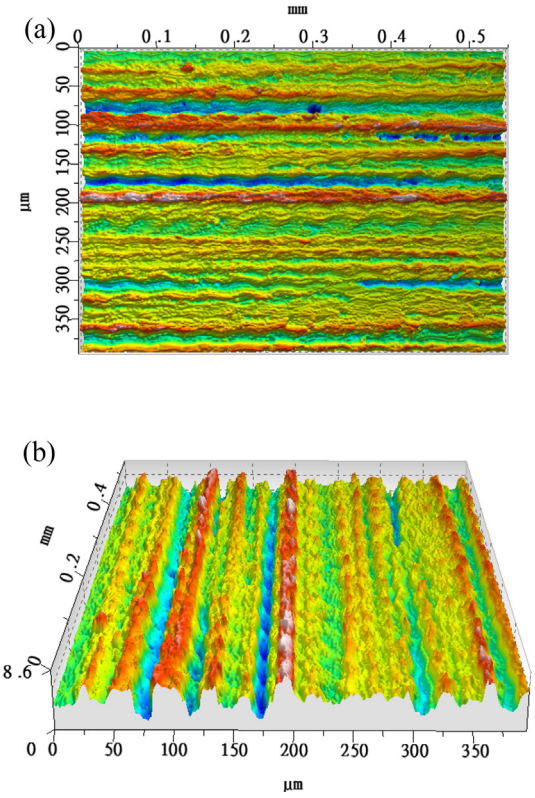

Fig. 15. Surface topography of the ultrasonic assisted grinding (a) overhead view; (b) 3-dimensional view.

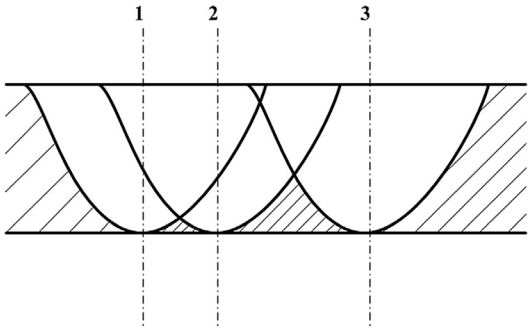

Fig. 16. Cross section of interference motion of abrasive particles in ultrasonic-assisted grinding process.

The interference motion of abrasive particles in ultrasonic-assisted grinding is further analyzed. Fig. 16 shows the cross section of interference motion of abrasive particles in the ultrasonic-assisted grinding process. As shown in Fig. 16, during the ultrasonic-assisted grinding process, the interference of three abrasive trajectories leads to a significant increase of the material removal rate and a decrease in the width and height of the grinding surface. That is to say, the surface roughness decreases and the surface height distribution is more concentrated, so that the surface has a stronger anti deformation ability and the contact stiffness of the workpiece surface improves.

6. Conclusion

(1) A new method of asperity definition based on the reference line and the height of peak and valley is proposed in this paper. The real profile of the rough surface is described by parabolas and they are simulated by ensuring the minimum least square error between the parabolas and the real profile. The contact analysis model of rough

surface is further obtained, which improves the accuracy of contact analysis.

(2) Under the experimental conditions, the surface contact performance of the workpiece is the best when the ultrasonic amplitude is 4 μm. The surface roughness of the workpiece is at least 24% lower than that of the conventional grinding surface. Under the same load, the surface contact stiffness of ultrasonic-assisted grinding surface is increased by at least 68%, and the maximum local contact pressure is reduced by at least 17%, which indicates a better contact fatigue performance.

(3) With the increase of cutting depth, the surface roughness of the workpiece increases. Under the same load, the contact stiffness decreases, and the maximum local contact pressure increases.

(4) With the increase of ultrasonic amplitude, the surface roughness decreases first and then increases. Under the same load, the contact stiffness increases first and then decreases, while the local maximum contact pressure presents an opposite variation trend. The contact performance of the ultrasonic-assisted grinding surface is not always better than that of the common grinding surface. In the case of larger ultrasonic amplitudes, the contact performance of the ultrasonic-assisted grinding surface is obviously decreases.

(5) It is found that under the appropriate ultrasonic amplitude, the mechanism of ultrasonic-assisted grinding to improve the contact performance of the workpiece surface is that the interference motion of abrasive particles makes the height distribution of the workpiece surface more concentrated and the density of asperity increased.

Acknowledgments

The authors gratefully acknowledge the support of the National Natural Science Foundation of China (NSFC) through Grants No. 51535012, U1604255, 51705142, the support of the Key research and development project of Hunan province through Grants No. 2016JC2001.

References

[1] S.Z. Wen, P. Huang, Principles of Tribology, Tsinghua University Press, Beijing, 2008.
[2] M. Renouf, F. Massi, N. Fillot, A. Saulot, Numerical tribology of a dry contact, Tribology International 44 (2011) 834–844.
[3] M. Kim, S.M. Lee, D.W. Lee, S. Park, S.H. Kim, Tribological effects of a rough surface bearing using an average flow analysis with a contact model of asperities, Int. J. Precis Eng. Man 18 (2017) 99–107.
[4] X.H. Meng, C.X. Gu, Y.B. Xie, Elasto-plastic contact of rough surfaces: a mixed-lubrication model for the textured surface analysis, Meccanica 52 (2017) 1541–1559.
[5] Kumabe Junichiro, The Foundation and Application of Precision Vibration Cutting, Machinery Industry Press, Beijing, 1985.
[6] A. Abdullah, A. Farhadi, A. Pak, Ultrasonic-assisted dry creep-feed up-grinding of superalloy inconel 738LC, Exp. Mech. 52 (7) (2012) 843–853.
[7] Y. Choi, K. Park, Y. Hong, et al., Effect of ultrasonic vibration in grinding; horn design and experiment, Int. J. Precision Eng. Manuf. 14 (11) (2013) 1873–1879.
[8] H. Chen, J. Tang, W. Zhou, An experimental study of the effects of ultrasonic vibration on grinding surface roughness of C45 carbon steel, Int. J. Adv. Manuf. Technol. 68 (9–12) (2013) 2095–2098.
[9] K.X. Xue, Study on Ultrasonic Griding Mechanism of Superalloy, Northeastern University, Shenyang, 2011.
[10] H. Chen, Study on Surface Forming Method and Mechanism of Surface Topography in Ultrasonic Grinding, Central South University, Changsha, 2015.
[11] K. Ding, Y. Fu, H. Su, et al., Wear of diamond grinding wheel in ultrasonic vibration-assisted grinding of siliconcarbide, Int. J. Adv. Manuf. Technol. 71 (9–12) (2014) 1929–1938.
[12] H. Chen, J. Tang, X. Lang, et al., Influences of dressing lead on surface roughness of ultrasonic-assisted grinding, Int. J. Adv. Manuf. Technol. 71 (2014) 2011–2015.
[13] T. Tawakoli, B. Azarhoushang, Influence of ultrasonic vibrations on dry grinding of soft steel, Int. J. Mach. Tools Manuf. 48 (14) (2008) 1585–1591.
[14] J.A. Greenwood, J.B.P. Williamson, Contact of nominally flat surfaces, Proc. R. Soc. A Math. Phys. 295 (1966) 300–319.
[15] Y.W. Zhao, D.M. Maietta, L. Chang, An asperity micro-contact model in corporating the transition from elastic deformation to fully plastic flow, J. Tribol.-Trans. ASME 122 (1) (2000) 86–93.
[16] D.J. Whitehouse, J.F. Archard, The properties of random surfaces of significance in their contact, Proc R. Soc. Lond. Ser. A 316 (1524) (1970) 97–121.
[17] J.A. Greenwood, J.J. Wu, Surface roughness and contact: an apology, Meccanica 36 (2001) 617–630.
[18] P. Pawlusa, W. Zelasko, The importance of sampling interval for rough contact mechanics, Wear 276 (2012) 121–129.
[19] E. Ciulli, L.A. Ferreira, G. Pugliese, S.M.O. Tavares, Rough contacts between actual engineering surfaces Part I: Simple models for roughness description, Wear 264 (11) (2008) 1105–1115.
[20] S. Kucharski, G. Starzynski, Study of contact of rough surfaces: modeling and experiment, Wear 311 (2014) 167–179.
[21] D. Tabor, The Hardness of Metals, Oxford University Press, Oxford, 1951.
[22] H. Chen, J. Tang, W. Shao, et al., An investigation on surface functional parameters in ultrasonic-assisted grinding of soft steel, Int. J. Adv. Manuf. Technol. (2018) 1–6.